Cancer Biol Med 2026. doi: 10.20892/j.issn.2095-3941.2025.0282

ORIGINAL ARTICLE

Migration and invasion inhibitory protein inhibits M2 macrophage polarization to suppress colorectal cancer progression through the STING–NFκB2–IL10 axis

Shuai Chen[1,2]*, Chenglu Lu[1,3]*, Jiaxin Li[1]*, Xilin Shen[1], Yan Sun[1]

[1]Department of Pathology, Tianjin Medical University Cancer Institute and Hospital, National Clinical Research Center for Cancer, Tianjin's Clinical Research Center for Cancer, Tianjin Key Laboratory of Digestive Cancer, Tianjin 300060, China; [2]Department of Pathology, Affiliated Hospital of Jining Medical University, Jining 272100, China; [3]Department of Pathology, Hebei Key Laboratory of Molecular Oncology, Tangshan People's Hospital, Tangshan 063000, China

ABSTRACT

Objectives: This study aimed to determine the role and mechanism underlying migration and invasion inhibitory protein (MIIP) modulation in M2 macrophages within the tumor microenvironment and the potential of targeting the MIIP– stimulator of interferon genes (STING) pathway in colorectal cancer (CRC) therapy.

Methods: MIIP expression was analyzed for associations with the STING pathway and M2 macrophage infiltration using public datasets and clinical CRC samples. CRC cells were genetically modified using lentiviral vectors to overexpress or silence MIIP and STING. The interactions of genetically modified CRC cells with macrophages were studied in co-culture systems. Techniques, including immunofluorescence staining, RT-qPCR, western blot, ELISA, flow cytometry, and Transwell migration and invasion assays, were used to evaluate the crosstalk between CRC cells and macrophages. An orthotopic mouse CRC model was developed to study the effects of MIIP on M2 macrophage polarization and tumor metastasis through the STING–NFκB2–IL10 axis. The therapeutic significance of a STING antagonist was also assessed *in vivo*.

Results: Analyses of The Cancer Genome Atlas (TCGA) cohort and our CRC cohort revealed low MIIP expression is associated with STING pathway activation, increased M2 macrophage infiltration, and poor clinical outcomes. The results of functional experiments demonstrated that MIIP inhibits IL10 production *via* the STING–TRAF3–NFκB2 axis in CRC cells, suppressing M2 macrophage polarization in co-culture systems. Conversely, M2 macrophages promoted CRC cell migration and invasion in an IL10-dependent manner. *In vitro* and *in vivo* studies confirmed that the MIIP-mediated feedback loop between CRC cells and macrophages depends on the STING–NFκB2–IL10 axis. Furthermore, inhibition of STING expression in a mouse model reduced M2 macrophage polarization and tumor metastasis.

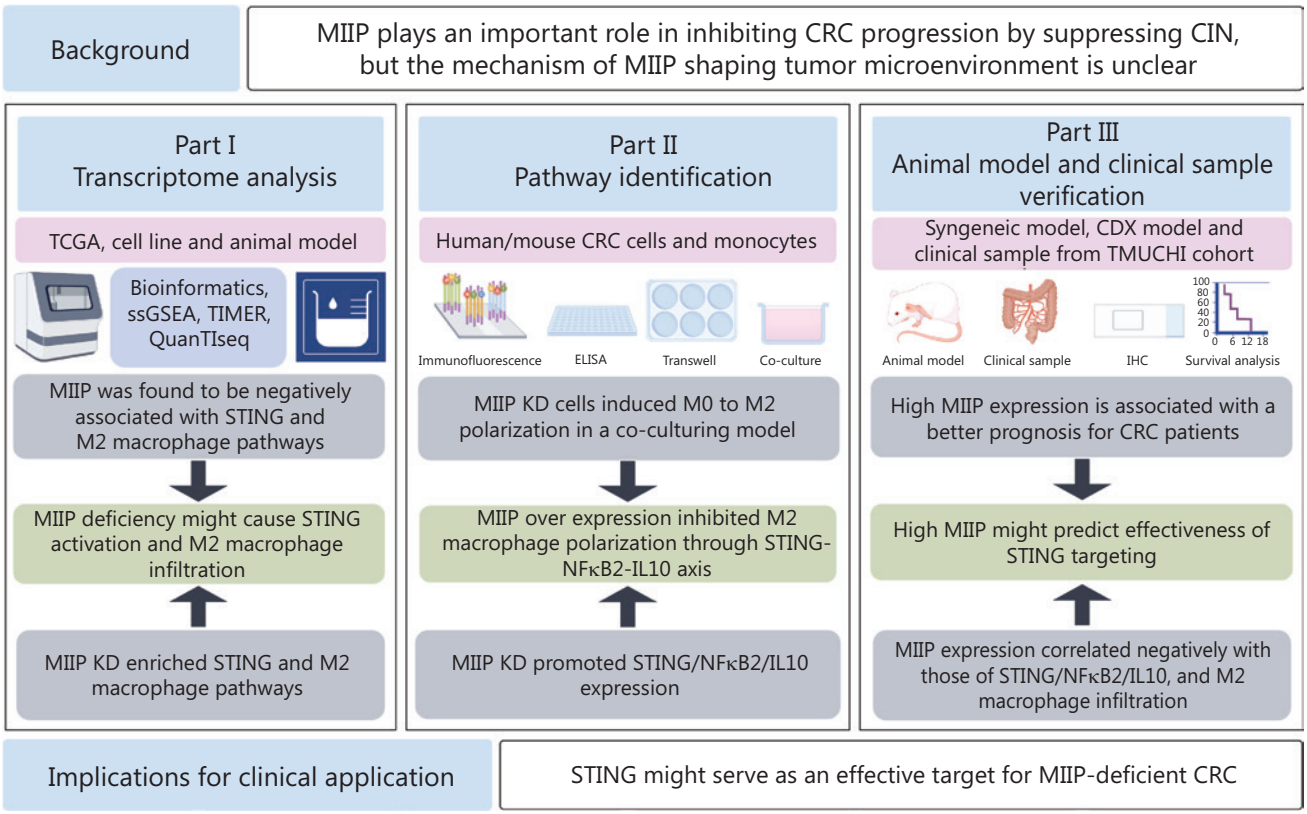
Conclusions: This study established MIIP as a crucial regulator of macrophage polarization in the CRC tumor microenvironment, providing new insights into the role in suppressing CRC progression and immune–tumor crosstalk. These findings highlight the potential of targeting the STING pathway as a therapeutic strategy for CRC patients who respond poorly to immune checkpoint inhibitors.

KEYWORDS MIIP; M2 macrophage; STING; IL10; colorectal cancer

Introduction

Colorectal cancer (CRC) ranks as the third most common malignancy and the second leading cause of cancer-related deaths globally according to GLOBOCAN 2022[1]. The 5-year survival rate for patients with advanced CRC in China is <20%, in large part due to disease recurrence and metastasis, despite comprehensive treatment strategies[2]. Immune checkpoint inhibitors (ICIs) have shown remarkable efficacy in various cancers, including CRC with microsatellite instability-high (MSI-H) or mismatch repair-deficient (dMMR) phenotypes, which account for <15% of all CRC cases[3-5]. However, patients with chromosomal instability (CIN), which represents approximately 85% of CRC cases, rarely benefit from ICI monotherapy. Combination therapies aimed at transforming "immune-cold" tumors into "immune-active" tumors may improve the therapeutic outcomes in these patients[5,6].

*These authors contributed equally to this work.
Correspondence to: Yan Sun
E-mail: sunyan@tjmuch.com
ORCID ID: https://orcid.org/0000-0001-8916-9598
Received May 25, 2025; accepted September 24, 2025;
published online January 14, 2026.
Available at www.cancerbiomed.org
©2026 The Authors. Creative Commons Attribution-NonCommercial 4.0 International License (CC BY-NC 4.0)



Flow chart of the study In our previous study we demonstrated that MIIP acts as a suppressor of colorectal cancer (CRC) progression by inhibiting chromosomal instability (CIN), yet the mechanism underlying remodeling the tumor microenvironment has not been elucidated. In Part I transcriptomic analyses across TCGA datasets, cell lines, and animal models of CRC revealed that downregulation of MIIP may activate the STING/NFκB pathway and induce M2 macrophage polarization. In Part II *in vitro* experiments demonstrated that MIIP inhibits M2 macrophage polarization through the STING–NFκB2–IL10 axis. In Part III *in vivo* and clinical analyses confirmed that MIIP restrains M2 macrophage polarization *via* the STING–NFκB2–IL10 axis and suggested that MIIP expression may serve as a predictive biomarker for the efficacy of STING-targeted therapy (created with Figdraw.com).

CIN in tumor cells has been shown to activate the cyclic GMP-AMP synthase–stimulator of interferon genes (cGAS-STING) signaling pathway through micronucleus formation, thereby influencing tumor immunity and progression[7-14]. Our previous research revealed that migration and invasion inhibitory protein (MIIP) haploinsufficiency substantially increases APC/C^{Cdc20} ubiquitin ligase activity and promotes overdegradation of cyclinB1, securin and TopoIIα, leading to weakened mitotic checkpoint activity, aberrant sister chromatid segregation, and deregulation of chromosomal topological stress, and consequently resulting in CIN[15]. These findings prompted us to investigate the effects of MIIP on the cGAS–STING pathway and tumor immunity in CRC.

In the current study low MIIP expression was shown to be correlated with elevated expression of STING, NFκB2, and IL10 with increased infiltration of M2 macrophages in CRC tissues. Moreover, low MIIP expression was associated with metastasis and shorter patient survival. Mechanistic studies revealed that MIIP downregulation increased the production of double-stranded DNA (dsDNA) in CRC cells, activating STING–NFκB2–IL10 signaling. Activation of the STING–NFκB2–IL10 signaling pathway promoted polarization of tumor-associated macrophages (TAMs) toward the M2 phenotype, which is characterized by high IL10 secretion. In turn, this positive feedback loop between MIIP-downregulated CRC cells and infiltrating M2 macrophages promoted CRC cell migration and invasion *in vitro* and facilitated tumor metastasis *in vivo*. Notably, these effects were mitigated by STING-targeted therapies, highlighting the therapeutic potential of targeting the STING–NFκB2–IL10 signaling pathway. This study revealed a novel mechanism by which MIIP modulates macrophages in the tumor microenvironment of CRC and influences tumor progression. Additionally, STING was identified as a promising therapeutic target for CRC patients with CIN who exhibit poor responses to ICIs.

Materials and methods

Bioinformatics analysis

RNA sequencing data were retrieved from The Cancer Genome Atlas (TCGA) database (https://www.cancer.gov/ccg/research/genome-sequencing/tcga). Functional enrichment data were obtained from the Comprehensive Analysis on Multi-Omics of Immunotherapy in Pan-cancer [CAMOIP][16] (http://www.camoip.net) and visualized in boxplots. Immune cell infiltration was analyzed using QuanTIseq[17] and TIMER 2.0[18] (http://timer.cistrome.org/). The samples were divided into two groups [high (H) and low (L) expression] based on the median level of *MIIP* expression.

Clinical samples

A total of 400 CRC tissue samples were collected from the Department of Pathology at Tianjin Medical University Cancer Institute and Hospital (Tianjin, China) between 2014 and 2018. These samples were designated the TMUCIH cohort. Tissue microarrays were constructed as previously described[15]. Clinicopathologic data from the 400 patients were also obtained. This study was approved by the Institutional Review Board of Tianjin Medical University Cancer Institute and Hospital (Approval No: EK201811) and informed consent was obtained from each patient.

Stable cell line establishment and cell culture

Human CRC cell lines (SW480, HCT116, and SW620), murine CRC cell lines (MC38 and CT26), and macrophage lines (THP-1 and RAW264.7) were obtained from the Cell Resource Center of the Chinese Academy of Medical Sciences (Beijing, China) and cultured as previously described[15,19,20]. Lentiviruses for human MIIP overexpression, murine MIIP overexpression, shMIIP (target sequence: 5′-GTGGAGGAAGACCATGAATGC-3′), and shSTING (target sequence: 5′-GCCCGGATTCGAACTTACAAT-3′) were obtained from Shanghai GeneChem Company (Shanghai, China). Lentivirus preparation and infection were performed as described previously[15]. Stable cell lines were generated through lentiviral infection and selection with puromycin. SW480-shMIIP cells were transfected with shSTING (SW480-shMIIP-shSTING) or a negative control lentivirus and selected with neomycin. Stable cell lines were validated by western blot analysis.

Cell co-culture

THP-1 cells were treated with PMA (100 ng/mL, 16561-29-8; Absin, shanghai, China) for 24 h to induce differentiation and the medium was replaced after the cells had adhered to the plate. THP-1 or RAW264.7 macrophages were seeded in the lower chamber of a Transwell system (3421; Corning, Tewksbury, MA, USA), while CRC cells (SW480, SW620, MC38, or CT26 cells) were seeded in the upper chamber. The medium was collected for ELISA after 48 h of co-culture. NeutraKine® IL-10 monoclonal antibody (10 ng/mL, 69018-1-Ig; Proteintech, Wuhan, Hubei, China), recombinant human IL-10 (10 ng/mL, HY-P70751; MedChemExpres, Monmouth Junction, NJ, USA), or recombinant mouse IL-10 (6 ng/mL, HY-P70517; MedChemExpres, Monmouth Junction, NJ, USA) was added to the lower chamber to assess the effect of IL-10. CRC cells were collected for Transwell migration and invasion assays after 48 h.

Immunofluorescence staining

Cells were seeded on coverslips in 6-well plates. The cells were fixed with 4% paraformaldehyde after 48 h, permeabilized with 0.3% Triton X-100, blocked with 3% BSA, and incubated with a primary antibody for 12–16 h at 4°C. The primary antibodies used included mouse anti-dsDNA (1:1000, ab270732; Abcam, Cambridge, MA, USA), rabbit anti-NFKB2/p52 (1:200, 15503-1-AP; Proteintech, Wuhan, Hubei, China), rabbit anti-TMEM173/STING (1:200, 19851-1-AP; Proteintech, Wuhan, Hubei, China), and rabbit anti-IL-10 antibodies (1:100, 20850-1-AP; Proteintech, Wuhan, Hubei, China). The cells were then incubated with secondary antibodies, including mouse IgG-AlexaFluor 488 (1:100, abs20014; Absin, Shanghai, China), mouse IgG-AlexaFluor 594 (1:100, abs20017; Absin, Shanghai, China), rabbit IgG-fluorescein [FITC] (1:100, SA00003-8; Proteintech, Wuhan, Hubei, China), rabbit IgG-Cy3 (1:1000, ab6939; Abcam, Cambridge, MA, USA), and rabbit IgG-Cy5 (1:1000, ab6564; Abcam), at room temperature. Formalin-fixed and paraffin-embedded (FFPE) tissue sections (4 μm) underwent similar staining procedures as previously described[21]. The tissues were incubated with rabbit anti-CD163 (1:100; 16646-1-AP; Proteintech, Wuhan, Hubei, China) and rabbit anti-MIIP antibodies (1:100, HPA044948; Sigma–Aldrich, St. Louis, MO, USA), followed by incubation for 1 h with rabbit IgG-CoraLite488 (1:100, SA00013-2; Proteintech, Wuhan, Hubei, China) and rabbit IgG-Cy3 antibodies (1:1000, ab6939; Abcam, Cambridge, MA, USA). Fluorescence images were captured using a BX51 fluorescence microscope (Olympus, Tokyo, Japan).

RNA isolation and quantitative RT–qPCR

RNA was extracted using TRIzol reagent (15596018CN; Invitrogen, Carlsbad, CA, USA). cDNA synthesis was performed with the Prime Script RT Reagent kit (RR037A; Takara, Tokyo, Japan). RT–qPCR was performed using TB Green® Premix Ex Taq GC (RR071B; Takara, Tokyo, Japan)

on a StepOne Plus Real-Time PCR system (4376600; Thermo, Waltham, MA, USA). The levels of expression were normalized to GAPDH and calculated using the $2^{-\Delta\Delta Ct}$ method. The primer sequences are provided in **Table S1**.

Western blot

Total protein was extracted using RIPA lysis buffer (9806; Cell Signaling Technology, Danvers, MA, USA) and separated by SDS-PAGE, after which the proteins were transferred onto PVDF membranes. The membranes were blocked with 5% BSA for 1 h at room temperature, followed by an overnight incubation with the primary antibodies at 4°C. The primary antibodies used included rabbit anti-MIIP (1:1000, HPA044948; Sigma-Aldrich, St. Louis, MO, USA), rabbit anti-MIIP (1:1000, orb537083; Biorbyt, Cambridge, UK), rabbit anti-STING (1:2000, 19851-1-AP; Proteintech, Wuhan, Hubei, China), mouse anti-TRAF3 (1:1000, 66310-1-Ig; Proteintech, Wuhan, Hubei, China), rabbit anti-p52 (1:1000, 4882S; Cell Signaling Technology, Danvers, MA, USA), rabbit anti-p52 (1:500, 15503-1-AP; Proteintech, Wuhan, Hubei, China), rabbit anti-p-p100 (1:1000, 4810T; Cell Signaling Technology, Danvers, MA, USA), rabbit anti-CD163 (1:1000, 68922; Cell Signaling Technology, Danvers, MA, USA), and mouse anti-β-actin antibodies (1:1000, 3700S; Cell Signaling Technology, Danvers, MA, USA). The membranes were then incubated with secondary antibodies, including mouse anti-rabbit IgG (1:5000, 3678; Cell Signaling Technology, Danvers, MA, USA) and rabbit anti-mouse IgG antibodies (1:5000, 58802; Cell Signaling Technology, Danvers, MA, USA), for 1 h at room temperature. The protein bands were visualized using a chemiluminescence detection system.

IL10 and CD163 detection with ELISA

IL10 and CD163 levels in cell culture supernatants or mouse serum were quantified using a human IL10 (abs510005; Absin, Shanghai, China), a human CD163 (ab100549; Abcam, Cambridge, MA, USA), a mouse IL10 (abs520005; Absin, Shanghai, China), and a mouse CD163 assay kit (ab255729; Abcam, Cambridge, MA, USA) according to the manufacturers' instructions.

Flow cytometry

The expression of CD206 on macrophage surfaces was analyzed by flow cytometry. Cells (4×10^5) were washed with PBS and stained with a mouse anti-FITC plus anti-human CD206 antibody (4 μL/test, FITC-65155; Proteintech, Wuhan, Hubei, China) for 30 min at room temperature in the dark. Flow cytometry analyses were performed using a FACSCanto™ II flow cytometer (Becton-Dickinson, Franklin Lakes, NJ, USA) and the results were analyzed with FACSDiva software (version 6.1.3).

Cell migration and invasion

Transwell assays were performed to assess cell migration and invasion. Matrigel-coated Transwell cell culture inserts were used for invasion assays. CRC cells (3×10^4 for migration and 5×10^4 for invasion) were seeded in serum-free medium in the upper chamber, while the lower chamber contained 10% FBS medium, VivaCell, Shanghai, China. or PMA-differentiated THP-1 or RAW264.7 macrophages. The migrated or invaded cells were stained and quantified after 48 h as previously described[22].

CRC xenograft and syngeneic mouse models

Male BALB/c nude mice (5 weeks old; SPF biotechnology, Beijing, China.) were randomized into 5 groups (n = 5 mice/group) and injected intracecally with 5×10^6 CRC cells in PBS. Treatments included shNC, shSTING, shMIIP, shMIIP+shSTING, or shMIIP and H151 (750 nmol/mouse injected every 2 d starting on day 22, 941987-60-6; MedChemExpres). The tumor volume was calculated using the formula, $V = (d^2 \times D)/2$, where d is the shortest and D is the longest diameter. The tumors and livers were collected for analysis.

Female BALB/c mice (SPF biotechnology, Beijing, China.) were similarly injected with CT26 CRC cells (5×10^6 cells in PBS) and treated with DMXAA (5 mg/kg dissolved in 100 μL of PBS daily starting on day 15, 117570-53-3; MedChemExpres, Monmouth Junction, NJ, USA). Tumor volume was determined and tissue handling was performed as described above. All procedures were approved by the Animal Ethics Committee of the Institute of Radiation Medicine [Chinese Academy of Medical Sciences, Beijing, China] (Approval No: IRM-DWLL-2020195).

RNA sequencing

Sequencing was performed by Novogene Corporation (Beijing, China). Total RNA was isolated from human CRC cell lines or mouse tumor tissue samples, followed by mRNA enrichment *via* poly-T oligo-attached magnetic beads. Sequencing libraries were prepared from the purified mRNA and subjected to paired-end (150 bp) sequencing on the Illumina HiSeq platform, San Diego, CA, USA. Raw reads were processed to quantify gene expression with read counts and normalized expression values (fragments per kilobase of transcript per million [FPKM] mapped reads) calculated using HTSeq (v0.6.0).

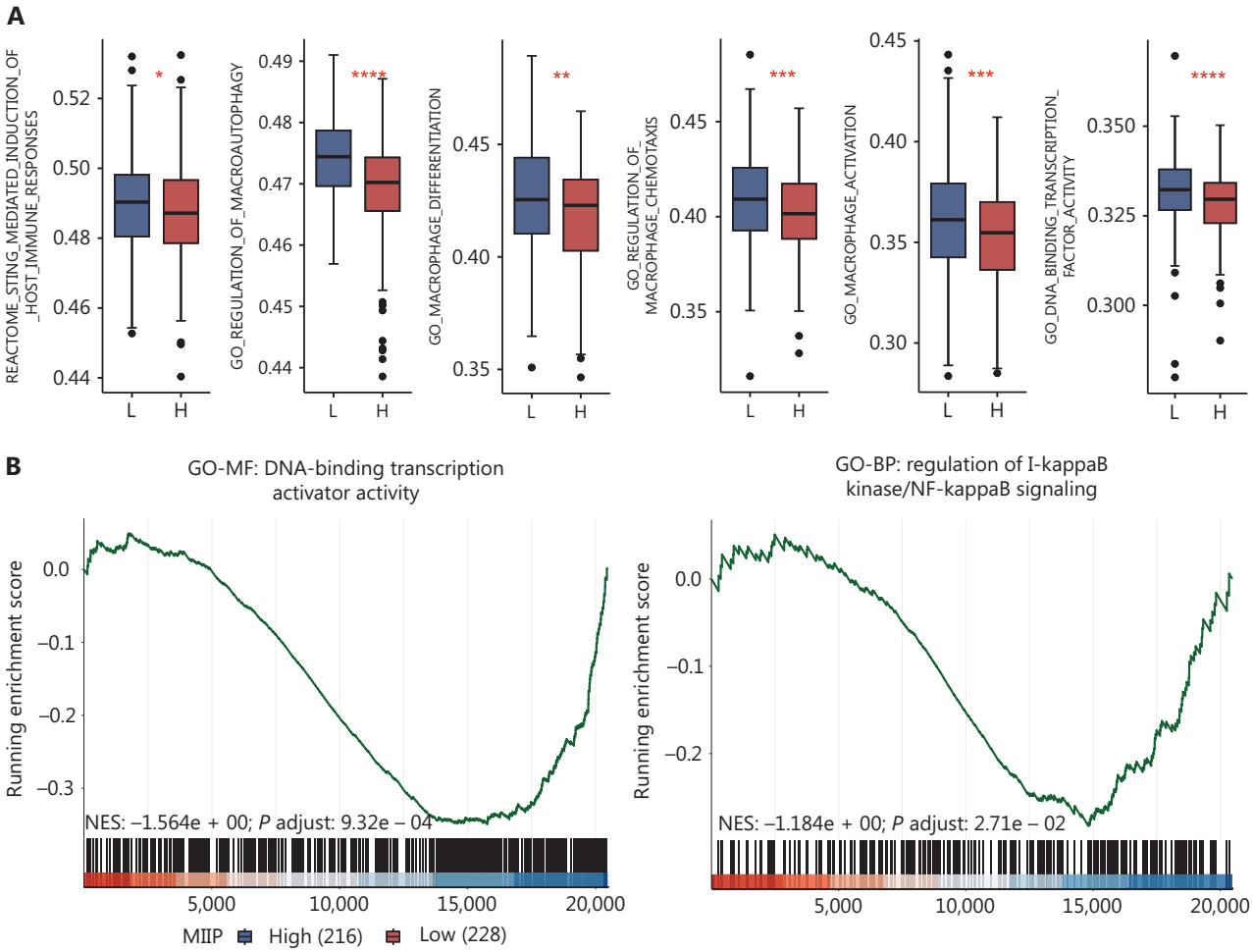


Figure 1 Continued

Immunohistochemical staining

FFPE tissue sections (4 μm) were stained using the EnVision two-step procedure and an IHC kit (PK10006; Proteintech, Wuhan, Hubei, China). The primary antibodies used included rabbit anti-MIIP antibody (1:200, 20630-1-AP; Proteintech, Wuhan, Hubei, China), rabbit anti-STING (1:4000, 19851-1-AP; Proteintech, Wuhan, Hubei, China), rabbit anti-NFκB2 (1:50, 15503-1-AP; Proteintech, Wuhan, Hubei, China), rabbit anti-IL10 (1:200, 20850-1-AP; Proteintech, Wuhan, Hubei, China), and rabbit anti-CD163 antibodies (1:2000, 16646-1-AP; Proteintech, Wuhan, Hubei, China). The process was executed according to the manufacturers' instructions, including the necessary positive and negative controls. IHC staining for the above biomarkers were evaluated by two independent pathologists as described previously[15,19-21]. The staining intensity and percentage of positive cells were scored (0–3) and total scores (0–9) were calculated to define high or low MIIP expression as described previously[15,23]. $CD163^+$ macrophage infiltration was quantified by manual counting in high-magnification fields (400×)[24].

Statistical analysis

All experiments were performed in triplicate and the data are presented as the means ± SDs. Statistical analyses were performed using GraphPad Prism V.7 and R (V.4.0.5). Details of the statistical tests are provided in the figure captions. A P value < 0.05 was considered to indicate statistical significance.

Results

Low MIIP expression is associated with a high level of STING pathway activity and M2 macrophage infiltration in CRC

Bioinformatics analyses were performed using the TCGA-colon adenocarcinoma (COAD) database. Single-sample gene set enrichment analysis (ssGSEA) revealed that immune-related pathways, including pathways involved in STING-mediated immune responses, macrophage activation, and

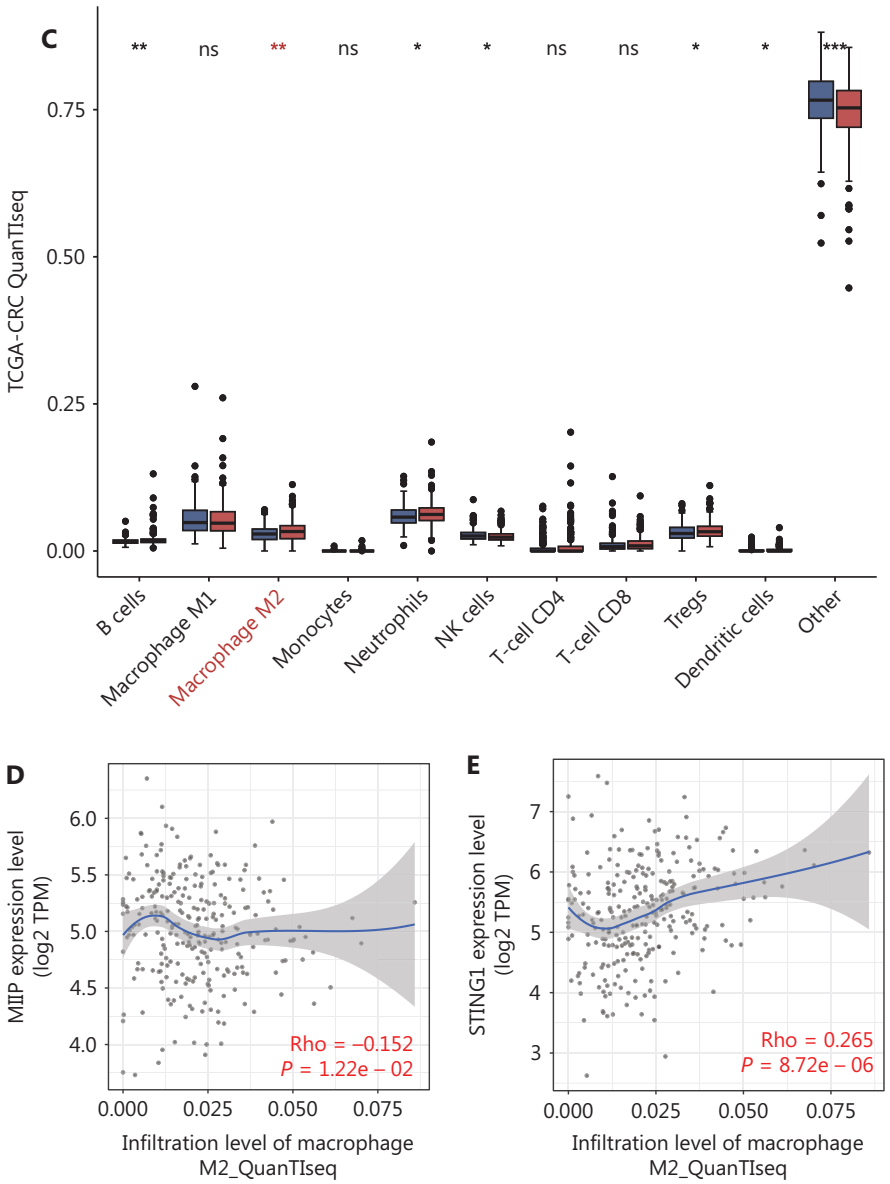


Figure 1 Bioinformatics analyses of MIIP expression, pathways, and immune cell infiltration in TCGA-CRC cohort. (A) ssGSEA shows the pathways with different enrichment scores between CRC samples with high (H) and low (L) MIIP expression, including STING-mediated induction of the host immune response, regulation of macrophage chemotaxis, macrophage activation, cell activation involved in the immune response, macrophage migration, and DNA-binding transcription activator activity. (B) GSEA reveals that MIIP-related genes are involved in DNA-binding transcriptional activity and the regulation of the I-kappaB kinase/NF-kappaB signaling pathways. (C) Comparison of immune cell populations between patients with high (H) and low (L) MIIP expression. (D) Scatter plot indicating the negative correlation between MIIP expression and M2 macrophage infiltration. (E) Scatter plot showing the positive correlation between STING1 expression and M2 macrophage infiltration. ns, not significant; *P < 0.05, **P < 0.01, ***P < 0.001, and ****P < 0.0001.

chemotaxis, were enriched in CRC patients with low MIIP expression (**Figure 1A**). GSEA further showed that low MIIP expression correlated with transcriptional activity linked to DNA binding and I-kappaB kinase/NF-kappaB signaling (**Figure 1B**). The analysis of immune cell infiltration using QuanTIseq revealed significant differences in the infiltration of B cells, M2 macrophages, neutrophils, NK cells, Tregs, and dendritic cells between CRC tumors with high MIIP expression and CRC tumors with low MIIP expression (**Figure 1C**). A subsequent correlation analysis indicated that MIIP expression was negatively correlated with M2 macrophage infiltration (P = 1.22e – 02; **Figure 1D**). The correlations between

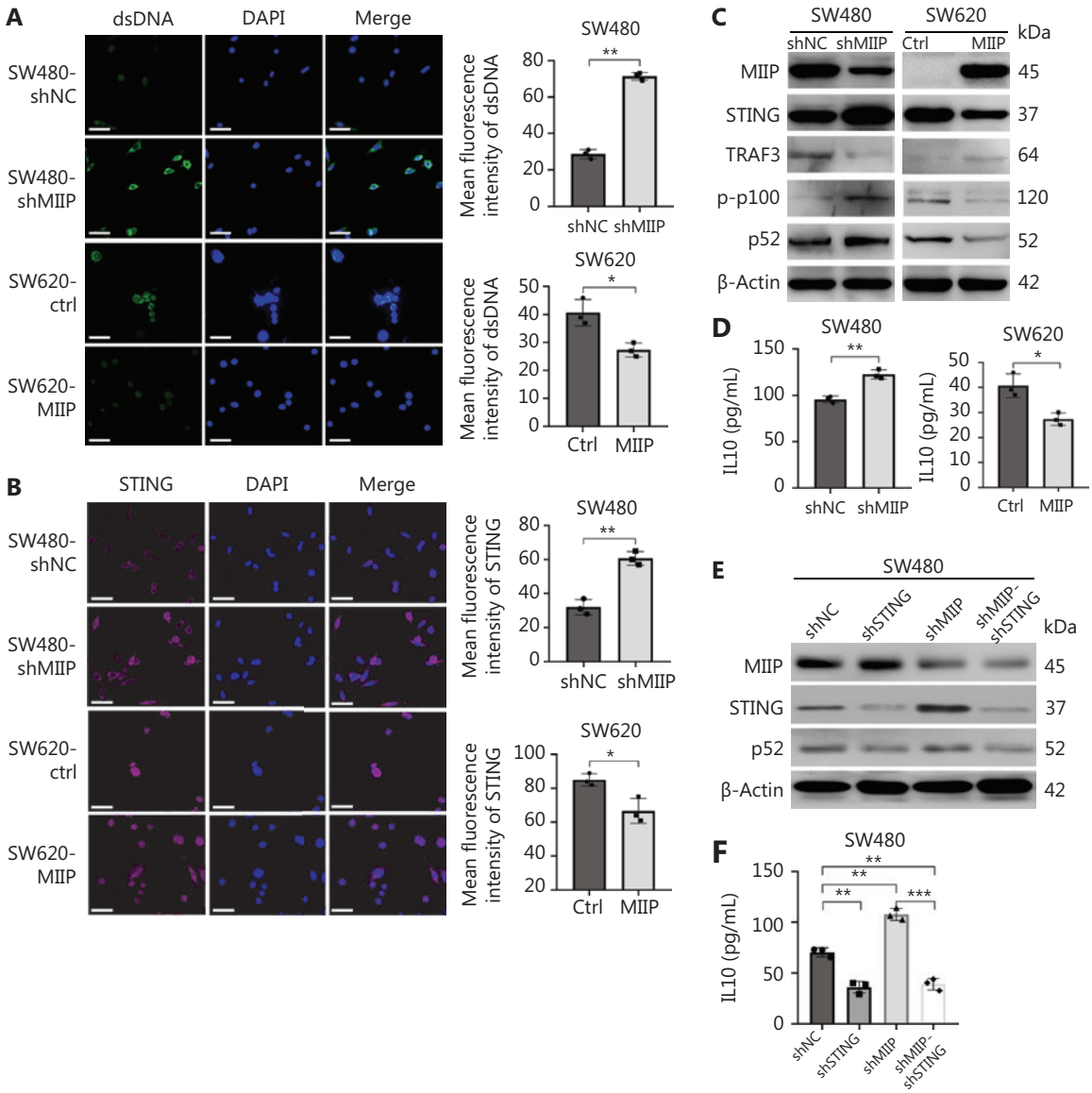


Figure 2 MIIP modulates the STING–NFκB2–IL10 signaling pathway in CRC cells. Immunofluorescence staining showing the effects of MIIP knockdown and MIIP overexpression on dsDNA levels (A) and the distribution and expression of STING (B) in SW480 and SW620 cells. (C) Western blots showing the effects of MIIP knockdown and overexpression on STING, TRAF3, p-p100, and p52 levels. (D) ELISA results showing the effects of MIIP knockdown and overexpression on IL10 levels in the cell culture medium. (E and F) Effects of MIIP knockdown and/or STING knockdown on p52 expression (E) and IL10 levels in the cell culture medium (F). All data are presented as the means ± SDs (n = 3). *P < 0.05, **P < 0.01, and ***P < 0.001; scale bar, 50 μm.

MIIP expression and infiltration of other immune cell types, including B cells, M1 macrophages, monocytes, neutrophils, NK cells, $CD4^+$ T cells, $CD8^+$ T cells, and DCs (but with the exception of Tregs [P = 0.0483]), were not significant (**Figure S1A–I**). In addition, STING1 expression was positively correlated with M2 macrophage infiltration (P = 8.72e − 06; **Figure 1E**). These findings suggest that MIIP downregulation activates the STING pathway and promotes M2 macrophage infiltration in CRC.

MIIP inhibits the STING–NFκB2–IL10 signaling pathway in CRC cells

RNA-seq was performed using human CRC cell lines with different levels of MIIP expression to confirm the findings from TCGA data. The NF-kappa B signaling pathway and regulation of DNA-binding transcription factor activity were enriched in HCT116-shMIIP cells (**Figure S2A**) and positive regulation of the NIK/NF-kappaB signaling pathway was enriched

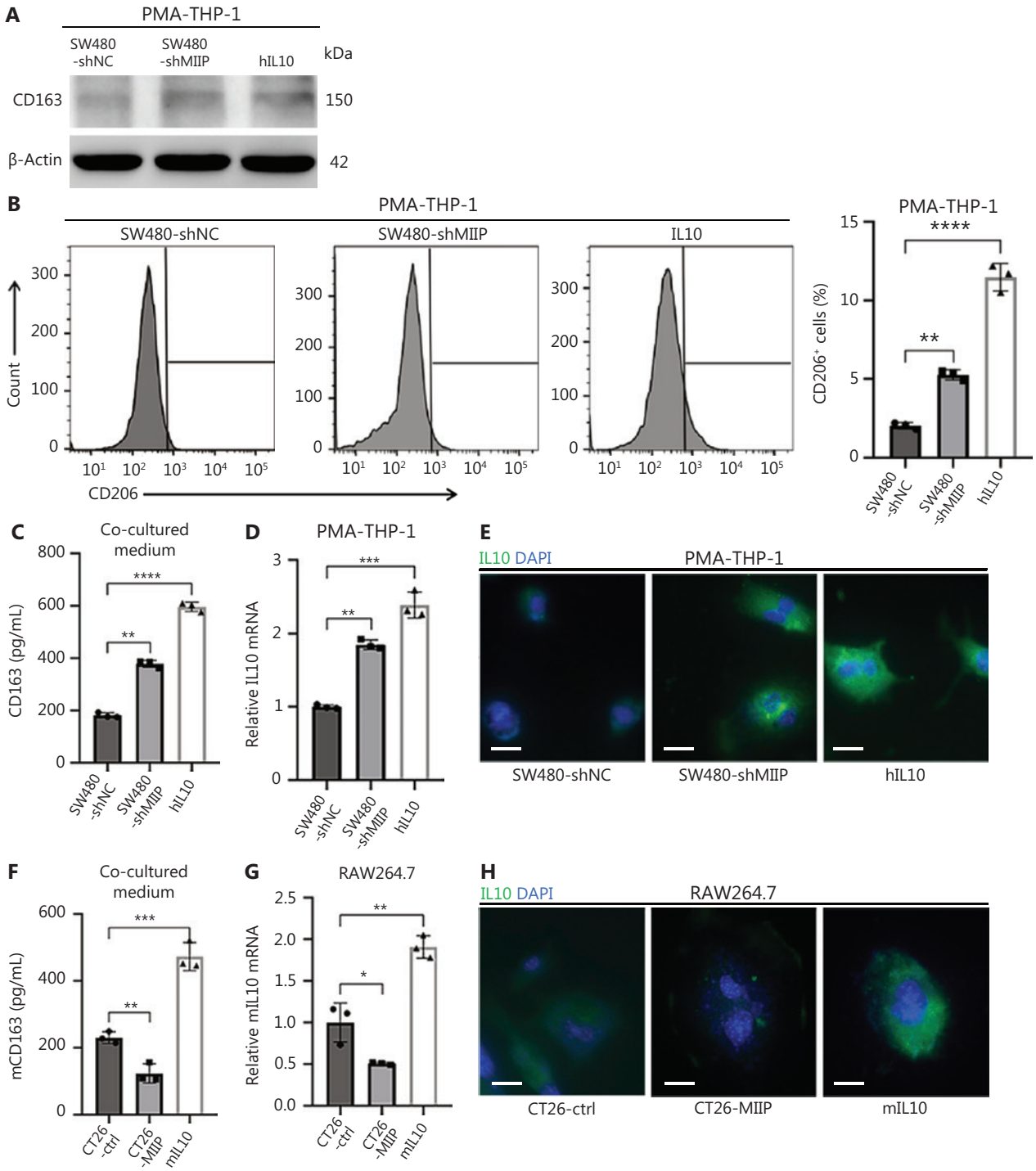


Figure 3 Continued

in SW480-shMIIP cells (**Figure S2B**). Immunofluorescence staining showed that MIIP knockdown increased cytoplasmic dsDNA levels and STING and nuclear p52 expression in SW480 cells, whereas MIIP overexpression reduced the levels in SW620 cells (**Figures 2A, B and S2C**). Western blot analysis demonstrated that MIIP knockdown increased STING expression, reduced TRAF3 expression, and increased p-p100 and p52 levels (**Figures 2C and S2D**). Conversely, MIIP overexpression decreased STING expression, increased TRAF3 expression, and decreased p-p100 and p52 levels (**Figure 2C**). Quantitative

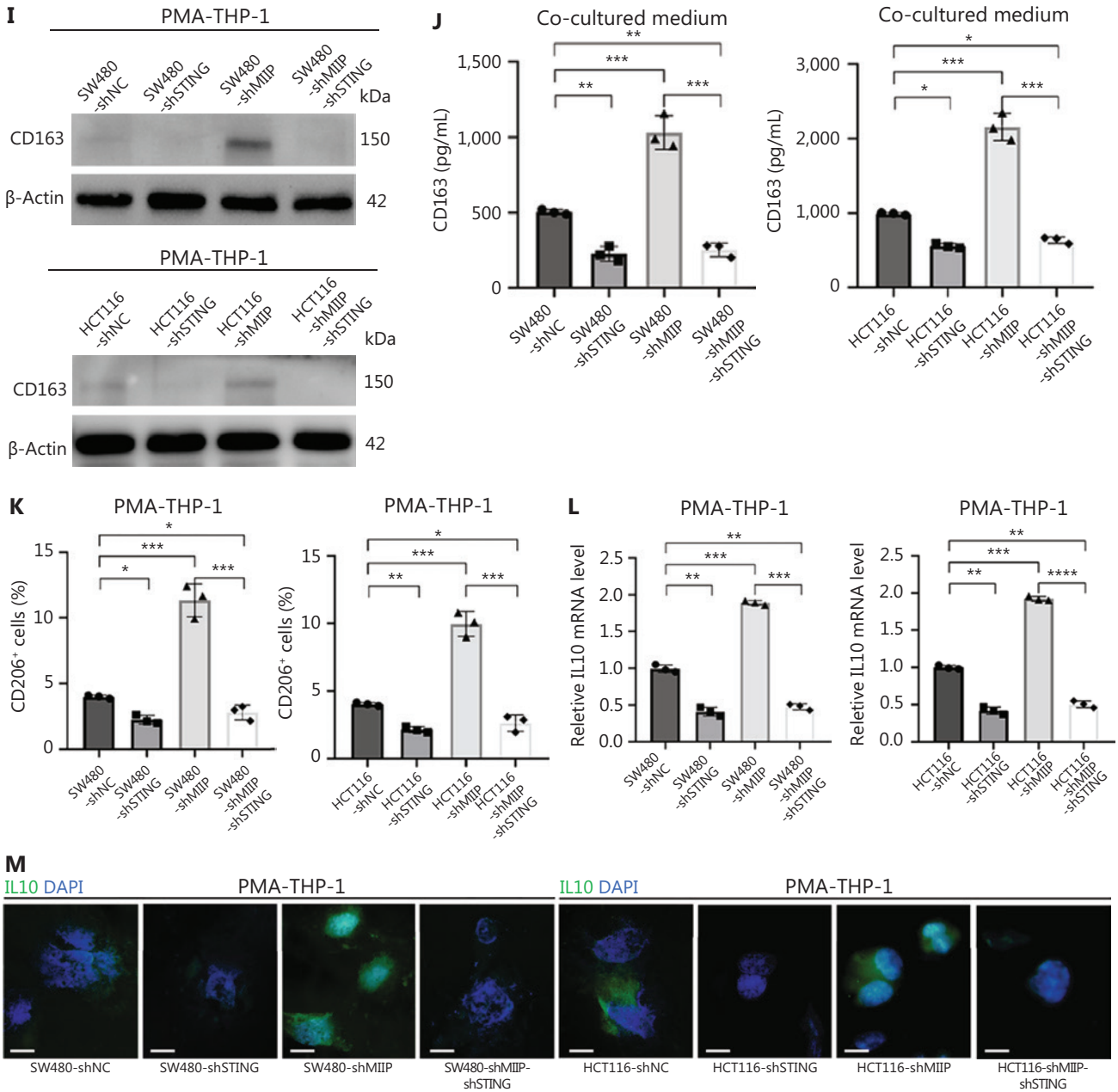


Figure 3 MIIP suppresses M2 macrophage polarization and decreases macrophage-derived IL10 levels in a co-culture system. MIIP knockdown in SW480 cells increased CD163 expression (A) and CD206 levels (B) in PMA-induced THP-1 cells, the CD163 level in the co-culture medium (C), the mRNA expression of IL-10 (D), and the IL10 levels (E) in PMA-induced THP-1 cells. MIIP overexpression in CT26 cells decreased the CD163 level in the co-culture medium of the co-cultured system (F) and macrophage-derived IL10 expression (G) and IL-10 levels in RAW264.7 cells (H). Effects of MIIP knockdown, STING knockdown, and dual MIIP and STING knockdown in CRC cells on CD163 expression in co-cultured PMA-treated THP-1 cells (I), CD163 levels in the co-culture medium (J), CD206 levels in PMA-treated THP-1 cells (K), and macrophage-derived IL10 expression (L) and IL-10 levels (M). All data are presented as the means ± SDs (n = 3). *P < 0.05, **P < 0.01, ***P < 0.001, and ****P < 0.0001; scale bar, 10 μm.

RT-qPCR showed that the transcription of IL10, but not IFN-β or IL6, was regulated by MIIP (**Figure S2E**). ELISAs revealed that MIIP knockdown significantly increased IL10 secretion (**Figures 2D and S2F**), whereas MIIP overexpression reduced IL10 levels in CRC cell culture medium (**Figure 2D**). MIIP and STING knockdown rescued the effects of MIIP on p52 expression and IL10 secretion (**Figure 2E, F**), which suggested that MIIP regulated IL10 production *via* the STING–NFκB2 axis.

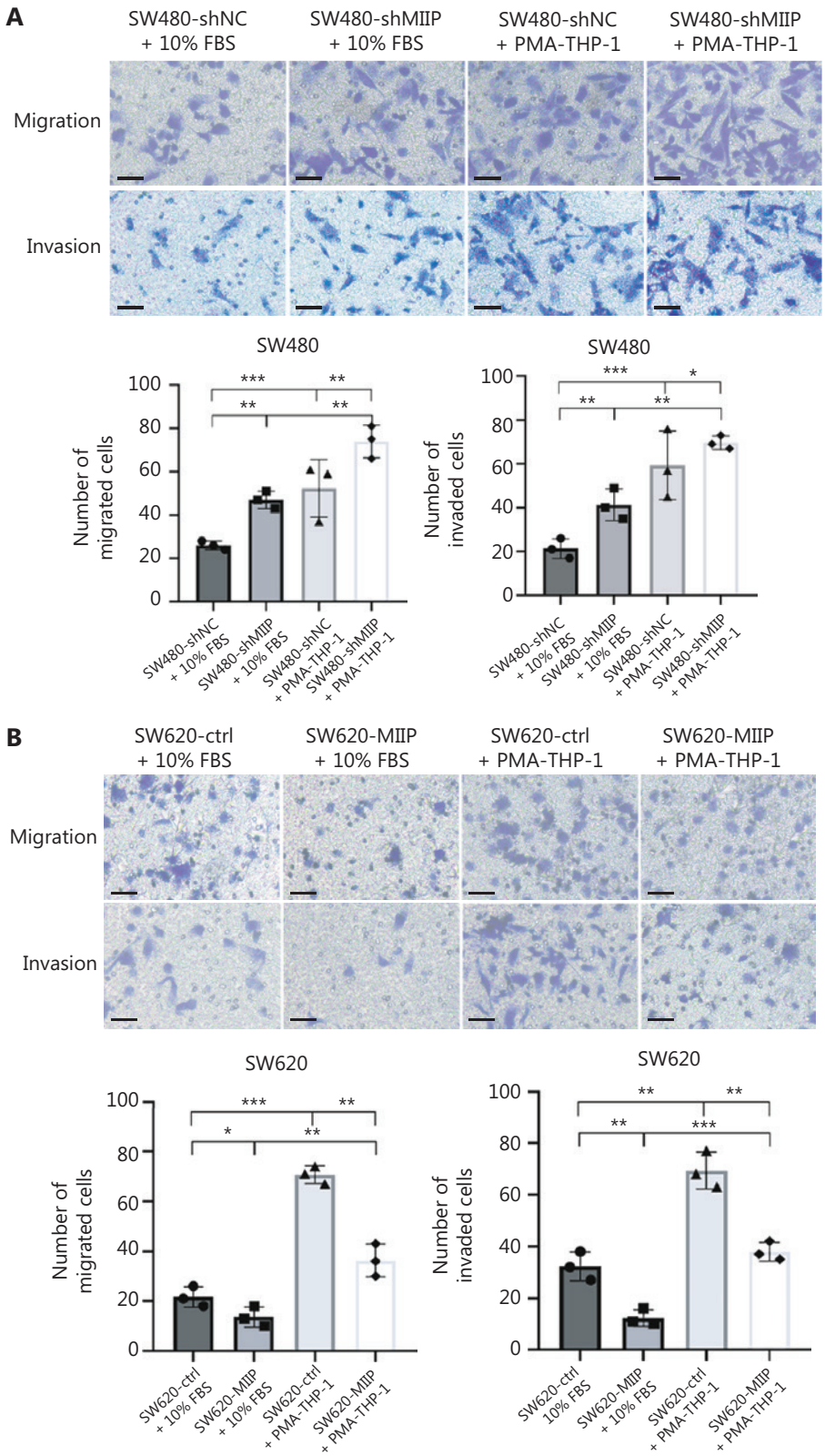


Figure 4 Continued

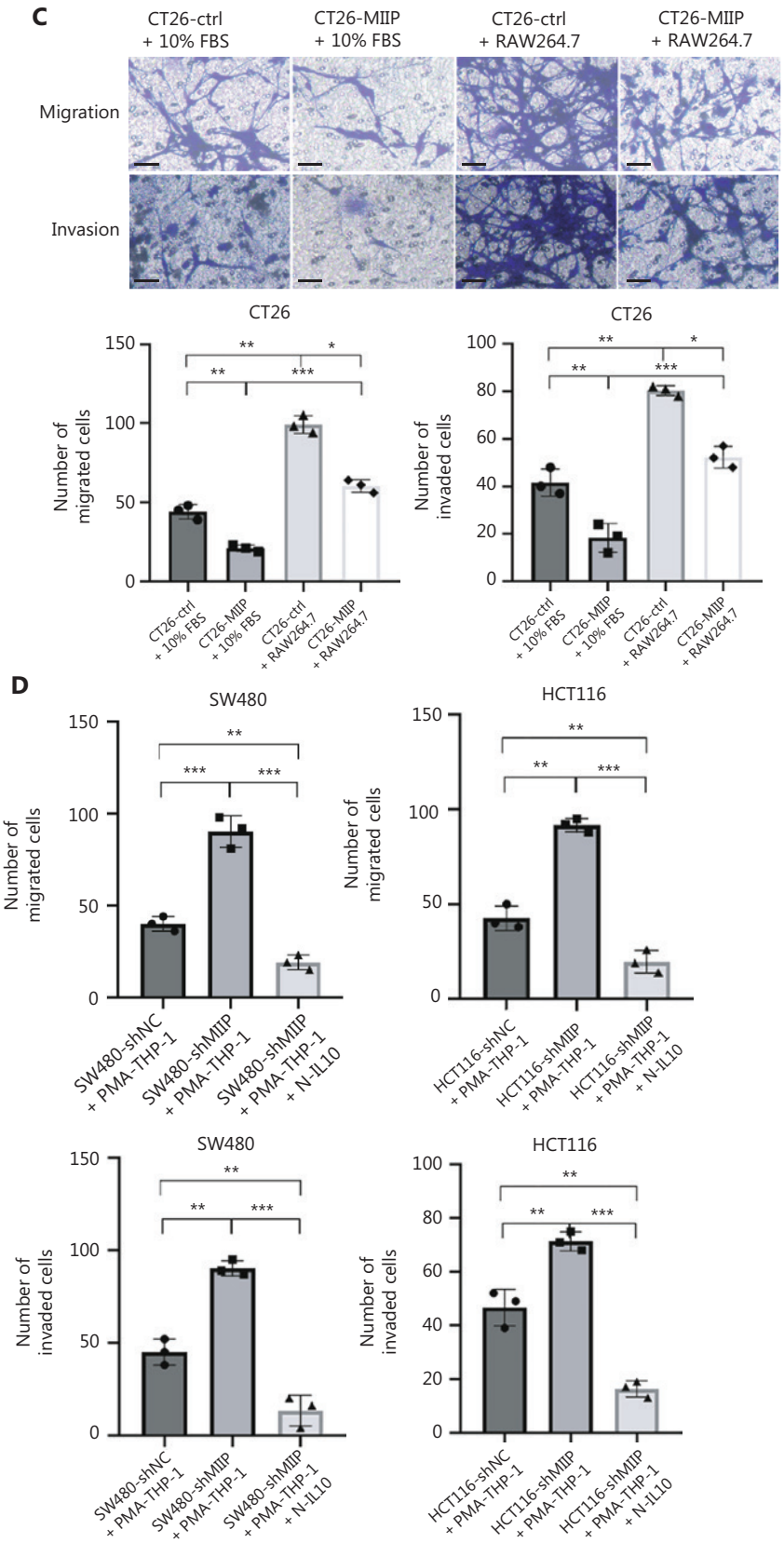


Figure 4 Continued

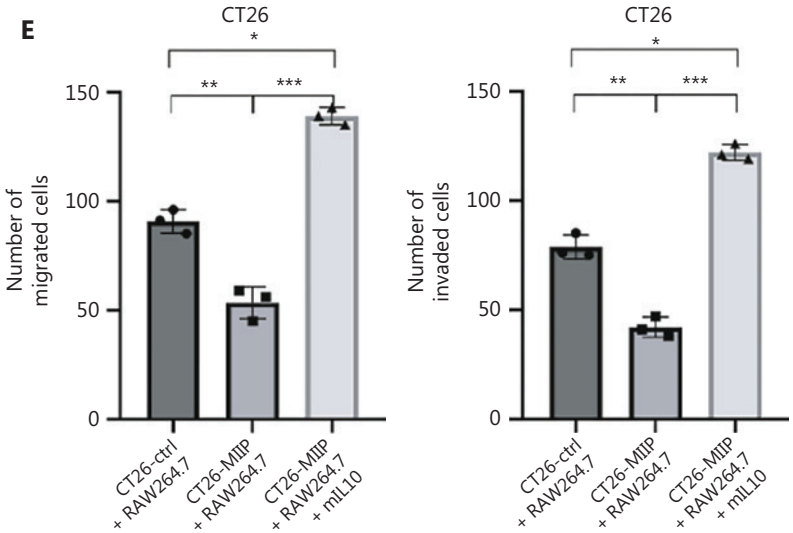


Figure 4 M2 macrophages promote the migration and invasion of CRC cells in a co-culture system through a mechanism dependent on IL10. Transwell migration and invasion assays showing the migration and invasion of SW480 (A) and SW620 (B) cells with different levels of MIIP expression and cultured with or without PMA-treated THP-1 cells. (C) Transwell migration and invasion assays revealed the migration and invasion of murine CRC cells (CT26) with different levels of MIIP expression and cultured with or without RAW264.7 cells. (D) Effect of N-IL10 in the co-culture system on CRC cell migration and invasion. (E) PMA-treated THP-1 cells and exogenous mIL10 influenced murine CRC cell migration and invasion, as shown by Transwell migration and invasion assays. The data are representative of at least three independent experiments and are presented as the means ± SDs (n = 3). *P < 0.05, **P < 0.01, and ***P < 0.001; scale bar, 50 μm.

MIIP suppresses M2 macrophage polarization and IL10 production *via* the STING pathway

A series of experiments was performed using a co-culture system to determine the effect of MIIP expressed in CRC cells on macrophages. MIIP knockdown in CRC cells increased CD163 and CD206 expression in PMA-treated THP-1 cells in the co-culture system (**Figures 3A, B and S3A, B**). ELISAs also demonstrated that MIIP knockdown in CRC cells increased CD163 levels in the co-culture medium (**Figures 3C and S3C**). In addition, MIIP knockdown in CRC cells promoted macrophage-derived IL10 expression (**Figures 3D, E and S3D, E**). Conversely, MIIP overexpression in CT26 cells decreased CD163 levels in the co-culture medium (**Figure 3F**) and macrophage-derived IL10 expression (**Figure 3G, H**). The combined knockdown of MIIP and STING in CRC cells reversed the effects of MIIP knockdown on macrophage polarization and IL10 production (**Figure 3I–M**), indicating that MIIP suppresses M2 macrophage polarization *via* the STING–NFκB2 axis.

M2 macrophages increase CRC cell migration and invasion in an IL-10-dependent manner

Transwell migration and invasion assays revealed that co-cultured M2 macrophages increased CRC cell migration and invasion, particularly in CRC cells with MIIP knockdown (**Figures 4A and S4A**). Conversely, MIIP overexpression in CRC cells inhibited migration and invasion, which were reversed by co-culture with M2 macrophages (**Figures 4B, C and S4B**). The addition of anti-IL10 antibodies inhibited the effects of MIIP on cell migration and invasion (**Figure 4D**), whereas exogenous IL10 restored the migration and invasion of MIIP-overexpressing cells (**Figure 4E**). These results indicated that IL10 has a key role in facilitating CRC cell aggressiveness in the tumor microenvironment.

The MIIP–STING–NFκB2–IL10 axis inhibits tumor growth and metastasis in mouse models

An orthotopic mouse CRC model was established using CT26 cells with different MIIP levels to assess tumor growth and liver metastasis (**Figure 5A**). The MIIP-overexpressing group had significantly reduced tumor sizes (**Figure 5B**), liver metastases (**Figure 5C**), and serum IL10 levels compared to the control group (**Figure 5D**). Conversely, a STING agonist (DMXAA) reversed these effects of MIIP (**Figure 5A–D**). Bulk RNA-seq was performed on tumor tissues from the CT-26-Ctrl and CT-26-MIIP groups. MIIP overexpression was shown to inhibit M2 macrophage infiltration and macrophage-related pathways, which is consistent with the RNA-seq results from TCGA data and human CRC cell lines (**Figure S5A, B**).

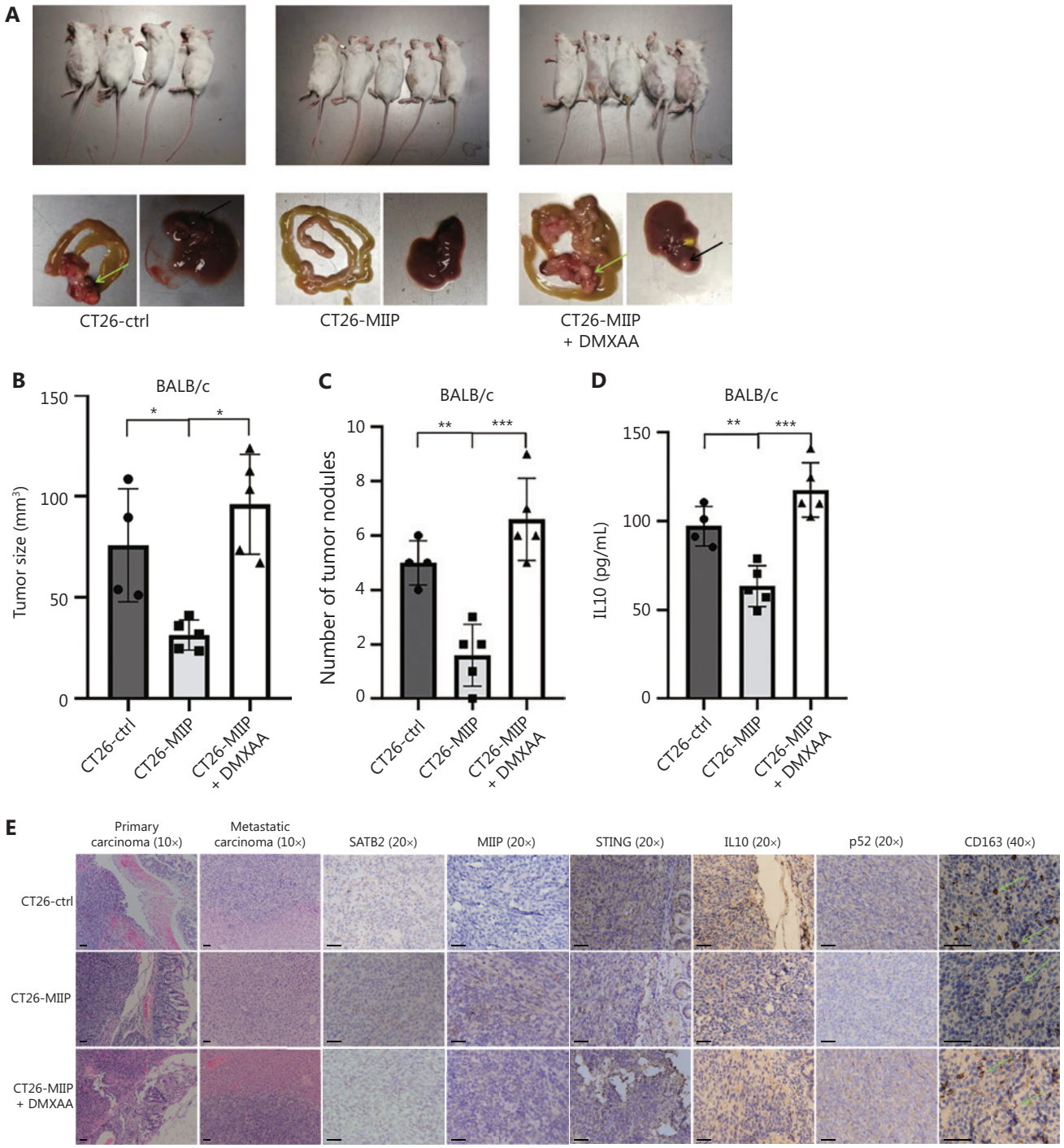


Figure 5 Continued

HE and immunohistochemical staining were performed for SATB2 (indicating CRC cells), MIIP, Ki-67, STING, p52, IL10, and CD163 in orthotopic tumor tissue samples. MIIP overexpression inhibited tumor cell proliferation, which is consistent with our previous study (**Figure S5C**). Moreover, MIIP overexpression led to a decrease in STING and p52 expression in CRC cells, a decrease in IL10 expression in tumor and stromal cells, and a decrease in the number of CD163-positive cells in tumor tissues compared to control treatment. The CT26-MIIP+DMXAA group presented increased p52 and IL10 expression and an increased number of CD163-positive cells compared to the CT26-MIIP group (**Figure 5D–I**). The *in vivo*

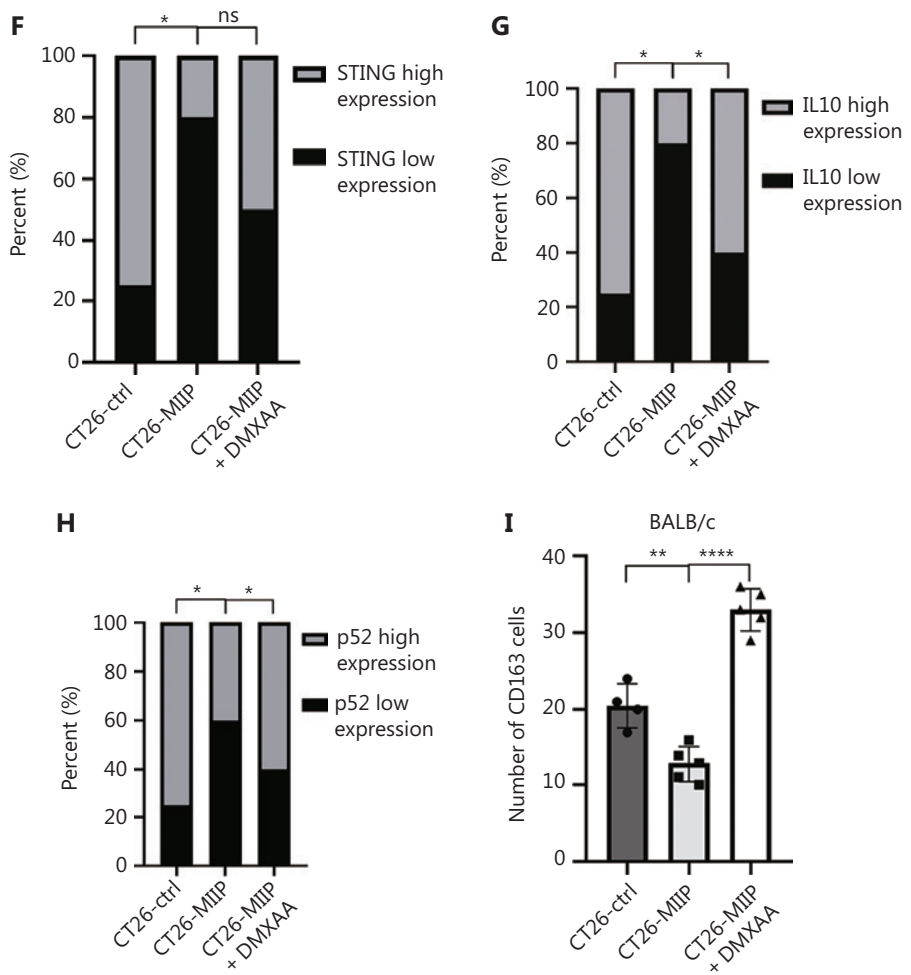


Figure 5 MIIP inhibits tumor growth and metastasis and M2 macrophage infiltration in a syngeneic CRC mouse model through the STING–NFκB2–IL10 axis. (A) Tumors *in situ* (indicated by green arrows) and liver metastatic nodules (indicated by black arrows) were observed in a syngeneic CRC mouse model. Statistics for the size of tumors *in situ* (B) and the number of metastatic foci (C). (D) Statistical analysis of IL10 levels in mouse blood. (E) Representative images of HE and IHC staining for SATB2, MIIP, STING, IL10, p52, and CD163 (green arrows) in tumor tissues from the different groups. The bar graphs show the percentages of high/low STING (F), IL-10 (G), and p52 (H) expression in the different groups. (I) Comparison of the number of CD163-positive cells among the different groups. All data are presented as the means ± SDs (n = 3). ns, not significant; *P < 0.05, **P < 0.01, ***P < 0.001, and ****P < 0.0001; scale bar, 50 μm.

results also confirmed that MIIP inhibits CRC progression and metastasis in part by modulating the STING–NFκB2–IL10 axis.

MIIP expression is negatively correlated with the STING axis and positively correlated with CRC patient survival

Immunohistochemical staining of 400 CRC tissue samples showed that low MIIP expression was associated with elevated STING, NFκB2, IL10, and CD163 levels (**Figure 6A**). Interestingly, even in the same tumor sample with intratumoral heterogeneity, negative correlations were noted between MIIP and STING, NFκB2, and IL10 expression (**Figure S6**). Immunofluorescence staining revealed that M2 macrophages were predominantly present in tumors with low MIIP expression (**Figure 6B**). In addition, strong correlations were identified between low MIIP expression and lymph node metastasis, distant metastasis, and an advanced TNM stage in CRC patients (**Figure 6C**). The survival analysis revealed that CRC patients with high MIIP expression experienced longer overall survival (OS) and progression-free survival (PFS) compared to patients with low MIIP expression (P = 0.005 and P = 0.048, respectively; **Figure 6D**).

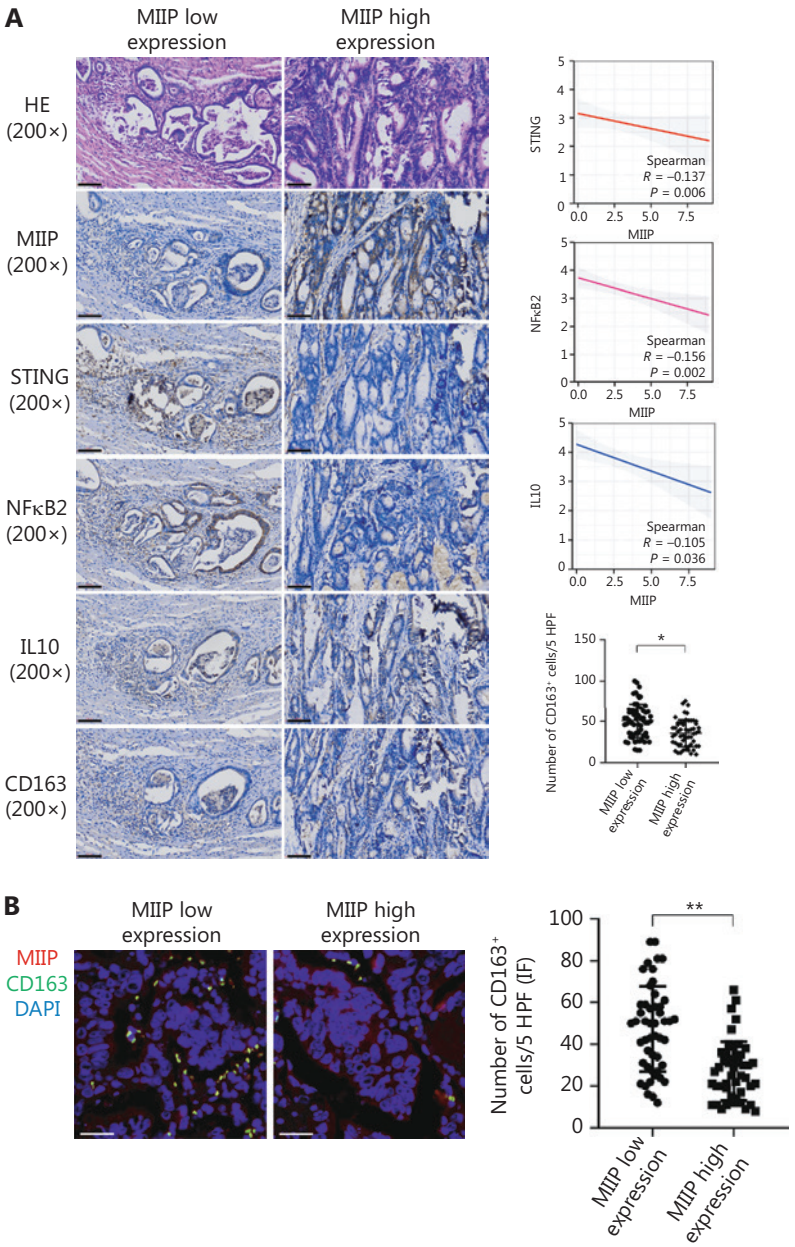


Figure 6 Continued

STING antagonists show therapeutic potential for CRC with low MIIP expression

An orthotopic nude mouse model was established using human CRC cell lines with different MIIP and STING levels, as well as a subgroup with STING-targeted drug (H151) treatment to explore the potential of STING antagonists as treatments for CRC. Tumorigenesis was detected in 66.7% of the control group (SW480-shNC), 25% of the STING-knockdown group (SW480-shSTING), 100% of the MIIP-knockdown group (SW480-shMIIP), 50% of the MIIP-STING double-knockdown group (SW480-shMIIP-STING), and 50% of the MIIP-knockdown with STING antagonist group (SW480-shMIIP+H151; **Figure 7A**). The tumor size was largest in the SW480-shMIIP group, smaller in the SW480-shMIIP-STING and SW480-shMIIP+H151 groups, and smallest in the SW480-shSTING group (**Figure 7B**). Moreover, more metastatic nodules were detected in the SW480-shMIIP group, fewer metastatic nodules were detected in the shMIIP-STING and SW480-shMIIP+H151

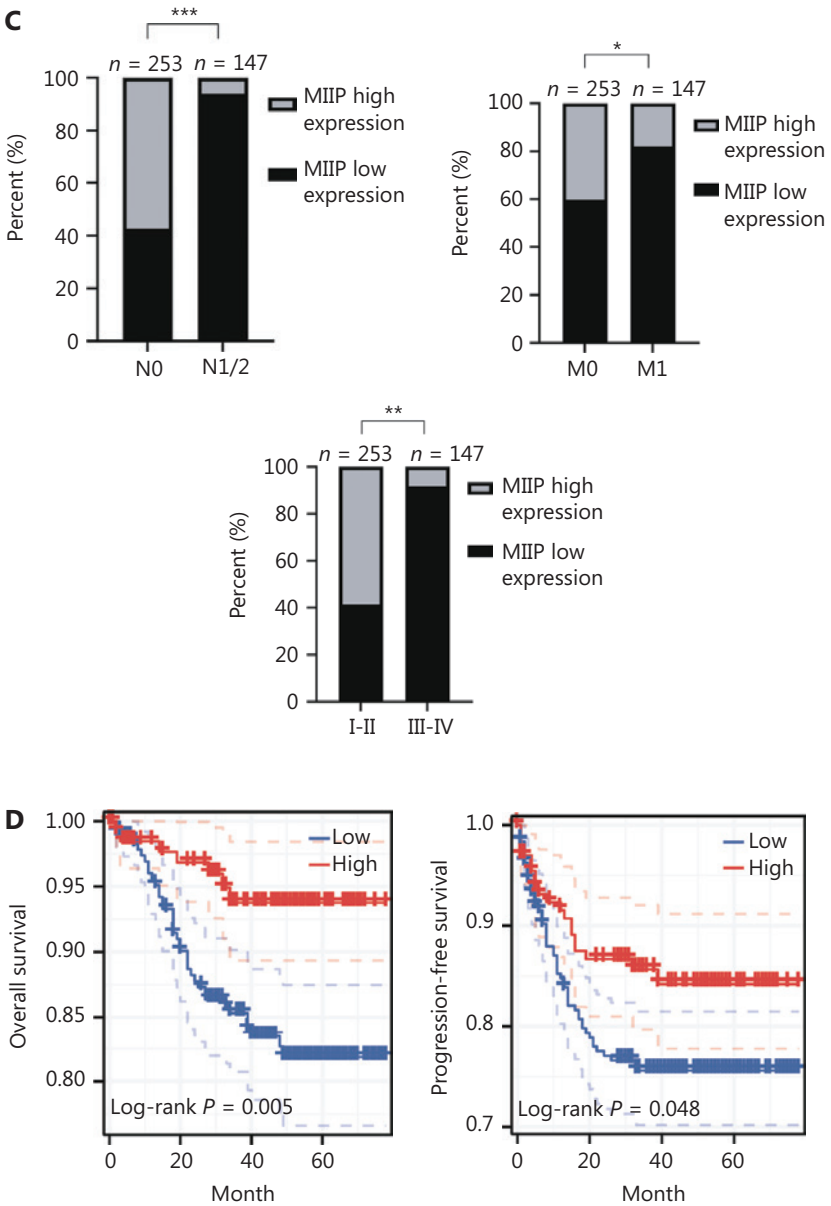


Figure 6 Relationships between MIIP expression and the STING immunologic pathway and survival of human CRC patients. (A) Representative images of H&E and immunohistochemical staining for MIIP, STING, NFκB2, IL10, and CD163 in CRC patients with low and high MIIP expression. The correlations among these markers and differences in the number of CD163-positive cells in the different groups are shown. (B) Representative images of IF staining for CD163 in CRC patients with low and high MIIP expression. The difference in the number of CD163-positive cells between the low- and high-MIIP-expressing groups was analyzed in 96 cases. (C) Relationships between MIIP expression and the M stage, N stage, and TNM stage of tumors. (D) Analysis of overall survival (OS) and progression-free survival (PFS) according to MIIP expression. *P* values were obtained using the log-rank test. All data are presented as the means ± SDs (n = 3). **P* < 0.05, ***P* < 0.01, and ****P* < 0.001; scale bar, 100 μm.

groups, and the fewest metastatic nodules were detected in the SW480-shSTING group (**Figure 7C**). These findings highlight the potential of STING antagonists as therapeutic agents for CRC characterized by MIIP downregulation.

Discussion

MIIP was first identified as an IGFBP-2 binding protein in glioma cells that inhibited glioma invasion and metastasis[25].

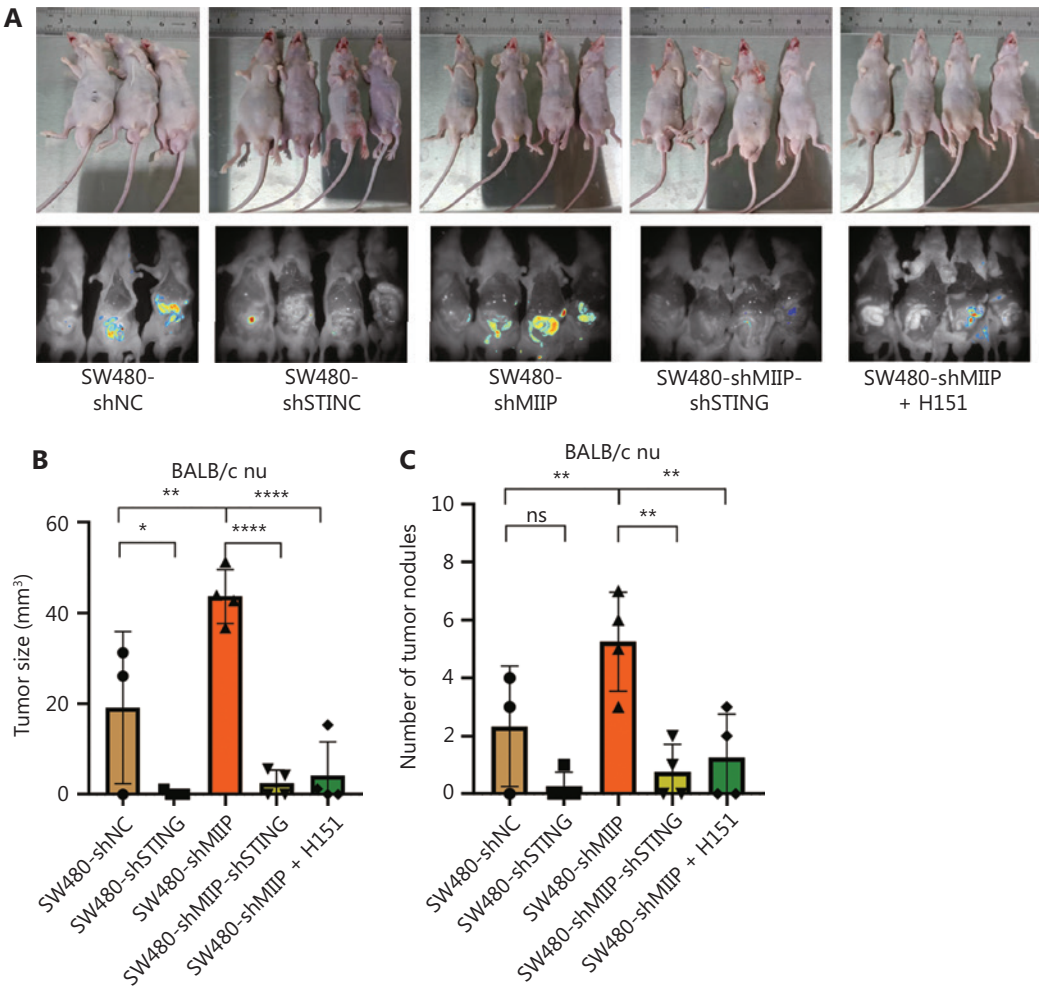


Figure 7 STING antagonist treatment in an orthotopic nude mouse model. (A) *In situ* CRC tumors and liver metastases in nude mice were observed using *in vivo* fluorescence experiments. (B and C) Statistics for the size of *in situ* tumors (B) and the number of metastatic foci (C). ns, not significant; **P* < 0.05, ***P* < 0.01, ****P* < 0.001, and *****P* < 0.0001.

Subsequently, MIIP was shown to exert tumor-suppressive effects by interacting with cell division cycle 20 homolog (CDC20) and histone deacetylase 6 (HDAC6) in gliomas[26,27] with Ras-related C3 botulinum toxin substrate 1 (Rac1) in endometrial cancer[28] and v-rel avian reticuloendotheliosis viral oncogene homolog A (RelA) in CRC[29]. In addition, MIIP inhibits the malignant progression of gastric cancer and hepatocellular carcinoma[30,31]. Recent studies have suggested that MIIP may also influence the tumor microenvironment. MIIP has been reported to inhibit cell proliferation and angiogenesis in clear cell renal cell carcinoma through the HIF-2α–CYR61 axis[32] and to suppress angiogenesis and tumorigenesis by interacting with ITGB3 in triple-negative breast cancer[33]. Moreover, downregulation of MIIP expression has been shown to drive CRC progression through the induction of peri-cancerous adipose tissue browning[34]. However, the role of MIIP in regulating the tumor immune microenvironment has not been investigated. In our previous study[15] we reported that MIIP haploinsufficiency induces high APC/C^{Cdc20} ubiquitin ligase activity and deregulation of Topo II activity, leading to CIN in CRC cells. In the current study MIIP downregulation was shown to increase IL-10 secretion *via* the dsDNA–STING–NFκB2–IL10 signaling axis in CRC cells and drive M2 macrophage polarization in the CRC tumor microenvironment. M2 macrophages in turn promote CRC cell migration and invasion in an IL-10-dependent manner (**Figure 8**). This is the first study to elucidate how MIIP-modulated crosstalk between CRC cells and the tumor immune microenvironment influences CRC progression.

Macrophages typically differentiate into two types (classic [M1 type] and alternative [M2 type] macrophages). M2 macrophages mainly express CD200R membrane glycoprotein

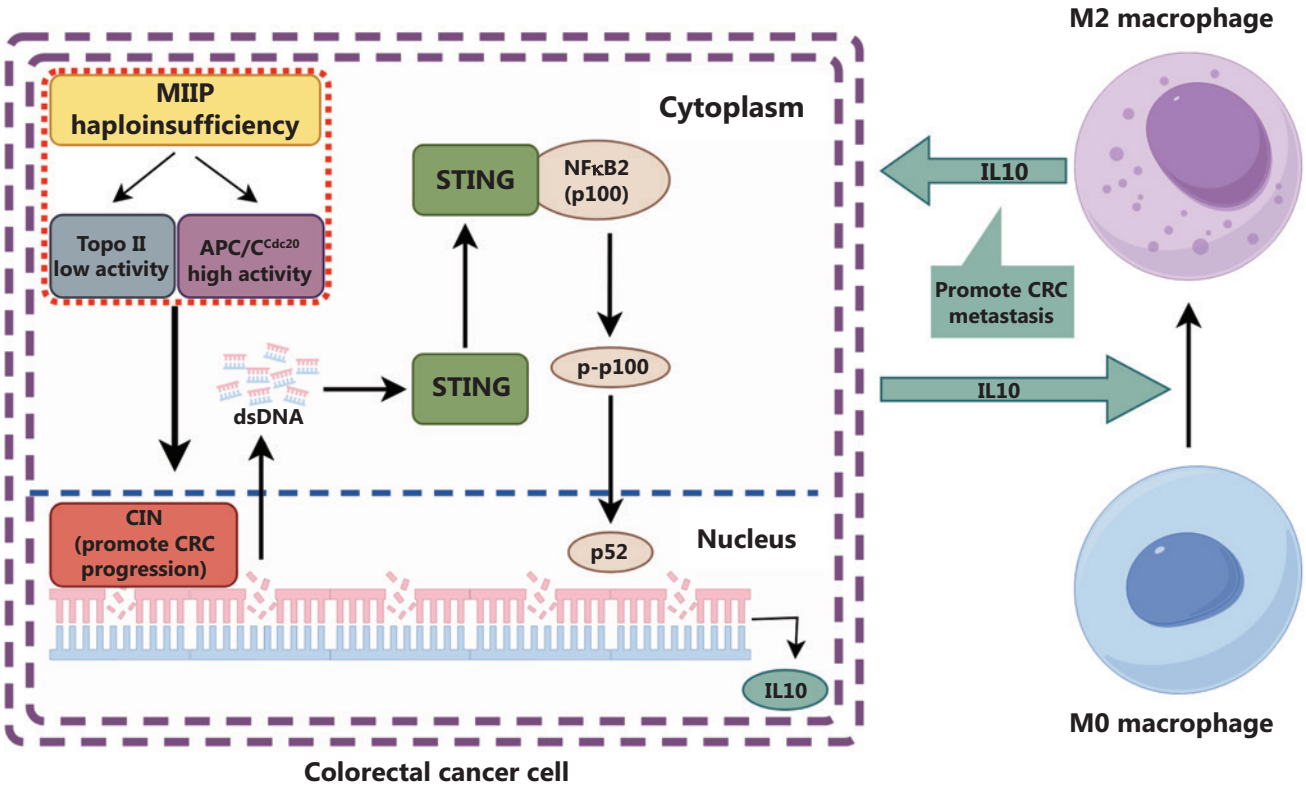


Figure 8 Schematic illustration of the mechanism by which MIIP haploinsufficiency promotes CRC progression through the modulation of CIN and M2 macrophage infiltration in the CRC microenvironment. In our previous study, MIIP haploinsufficiency was shown to induce excess APC/C^{Cdc20} ubiquitin ligase activity and the deregulation of Topo II activity, leading to CIN in CRC cells (in the red dotted line). The results of the current study further revealed that MIIP downregulation increases IL10 secretion *via* the dsDNA–STING–NFκB2–IL10 signaling axis in CRC cells and drives M2 macrophage polarization in the CRC tumor microenvironment. M2 macrophages promote CRC cell migration and invasion in turn in an IL-10-dependent manner (created with Figdraw.com). APC/C, anaphase-promoting complex/cyclosome; MIIP, migration and invasion inhibitory protein; CIN, chromosomal instability; STING, stimulator of interferon genes; CRC, colorectal cancer.

(CD163) and macrophage mannose receptor (CD206) on the surface[35-37]. M2 macrophages contribute to multiple oncogenic processes, including promotion of cancer cell proliferation, facilitation of neoangiogenesis and lymphangiogenesis, induction of the epithelial-to-mesenchymal transition (EMT), remodeling the extracellular matrix to support metastasis, and shaping the TME into an immunosuppressive state[38-40]. In this study, M2 macrophages were shown to increase CRC cell migration and invasion using a Transwell co-culture system. Moreover, *in vitro* and *in vivo* evidence was provided showing that MIIP downregulation partially inhibits CRC progression through M2 macrophages in CRC. However, considering that MIIP can inhibit CRC progression through intrinsic regulation of tumor cell proliferation, migration, and invasion, studying MIIP-mediated crosstalk between CRC cells and macrophages at different stages of CRC progression or under different host conditions is warranted in the future.

M2 macrophages have been shown to facilitate tumor invasion and metastasis through upregulation of anti-inflammatory cytokine and chemokine expression, such as IL-10, TGF-β, and chemokine ligands[41-43]. Liu et al. reported that Wnt5a-induced M2 polarization of tumor-associated macrophages *via* IL-10 promotes CRC progression[44]. In the present study M2 macrophages promoted the migration and invasion of CRC cells, which could be inhibited by a neutralizing antibody against IL-10. Although MIIP overexpression reduced the migration and invasion of CRC cells, recombinant IL10 protein increased the migration and invasion of CRC cells. In contrast, M2 macrophages are activated by IL10 and IL13 in CRC[45,46]. Sun et al. reported that exosomal circPOLQ promotes macrophage M2 polarization by activating the IL-10/STAT3 axis in a CRC model[47]. The results herein not only highlighted the roles of IL-10 in M2 macrophage polarization and CRC metastasis but also indicated that MIIP inhibits M2 macrophage polarization and CRC metastasis through IL-10. However, the origin of IL-10 in the co-culture system has not been specifically distinguished, so the effects of IL-10 on CRC cells or macrophages with different labels will be distinguished in the future.

An et al. recently reported that STING expression is significantly upregulated in CRC tissues and is positively correlated with macrophage density[48]. In agreement with these findings, STING1 expression was positively correlated with M2 macrophage infiltration in CRC samples from TCGA cohort and a positive correlation was confirmed between STING1 expression and M2 macrophage infiltration in a CRC mouse model and CRC samples from the TMUCIH cohort in this study. MIIP downregulation was confirmed to increase dsDNA levels and activate the STING pathway in the present study. This finding is consistent with our previous study in which we showed that *MIIP* haploinsufficiency induces CIN[15], which could activate the cGAS–STING pathway[49]. STING has been reported to activate noncanonical NFκB signaling in the immune response and ChIP assays have verified that IL10 is regulated by noncanonical NFκB signaling[50-55]. Accordingly, MIIP-mediated STING activation was shown to increase the levels of p-p100 and p52 protein as well as p52 nuclear translocation, indicating the activation of noncanonical NF-κB signaling. Moreover, STING activation increased the IL-10 mRNA and protein levels. Based on the literature and our results, we propose that MIIP regulates IL10 secretion through the STING–NFκB2 axis, which was confirmed by the interference of STING blocking the effects of MIIP *in vitro* and *in vivo*. This report is the first to show that MIIP regulates macrophages in the tumor immune microenvironment through the STING–NFκB2–IL10 axis and inhibits CRC invasion and metastasis through a feedback loop. However, the detailed modulatory mechanism warrants further investigation.

The dual role of the STING pathway in cancer remains complex. While STING agonists, such as DMXAA, have been shown to reduce tumor growth in breast cancer models[56,57], STING agonists may also promote rapid T-cell apoptosis and tumor progression under some conditions, particularly in CIN tumors[14,58]. In the current study continuous low-dose DMXAA treatment exacerbated tumor growth and metastasis in MIIP-overexpressing CRC, suggesting a tumor-promoting role for STING under specific circumstances. Conversely, the STING antagonist, H151, effectively reduced tumor growth and metastasis in CRC models, consistent with the reported benefits in breast cancer and melanoma[59]. These findings underscore the need for further investigation into the context-dependent effects of STING modulation before clinical application.

Grant support

This work was supported by grants from the National Natural Science Foundation of China [Grant No. 81871990 (Yan Sun)], the Key Project of Tianjin Natural Science Foundation [Grant No. 24JCZDJC00320 (Yan Sun)], the Key Project in 14th Five-Year Plan Special for Cancer Prevention and Treatment Research from Tianjin Cancer Institute [Grant No. YZ-06 (Yan Sun)], the Construction Project of Cancer Precision Diagnosis and Drug Treatment Technology from TUCIH [Grant No. ZLJZZDYYWZL13 (Yan Sun)], Tianjin Key Medical Discipline (Pathology) Construction Project [Grant No. TJYXZDXK-3-016C (Yan Sun)], Jining City Key Research and Development Program Project [Grant No. 2023YXNS062 (Shuai Chen)] and Jining Medical University Affiliated Hospital Talent Doctoral Research Fund Project [Grant No. 2024-BS-006 (Shuai Chen)], and Tangshan Science and Technology Project [Grant No. 2025150220C (Chenglu Lu)].

Conflict of interest

The authors have no conflicts of interest to declare.

Author contributions

Performed study design and authorized the manuscript: Yan Sun.
Performed experiments, analyzed data, and wrote the manuscript: Shuai Chen and Chenglu Lu.
Performed IHC and animal experiments: Jiaxin Li.
Performed bioinformatics analysis: Xilin Shen.

Data availability statement

Data on functional enrichment were obtained from the webtool for Comprehensive Analysis on Multi-Omics of Immunotherapy in Pancancer (CAMOIP, http://www.camoip.net) and visualized *via* boxplots. QuanTIseq was used to analyze the differences in immune cell infiltration between the high- and low-expression groups of MIIP and the TIMER 2.0 (http://timer.cistrome.org/) database was utilized to examine the correlation between TMEM173 transcription levels and macrophage infiltration scores. All other raw data and the data generated in this study are available upon request from the corresponding author.

References

1. Bray F, Laversanne M, Sung H, Ferlay J, Siegel RL, Soerjomataram I, et al. Global cancer statistics 2022: GLOBOCAN estimates of incidence and mortality worldwide for 36 cancers in 185 countries. CA Cancer J Clin. 2024; 74: 229-63.
2. Rawla P, Sunkara T, Barsouk A. Epidemiology of colorectal cancer: incidence, mortality, survival, and risk factors. Prz Gastroenterol. 2019; 14: 89-103.
3. Conche C, Finkelmeier F, Pešić M, Nicolas AM, Böttger TW, Kennel KB, et al. Combining ferroptosis induction with MDSC blockade renders primary tumours and metastases in liver sensitive to immune checkpoint blockade. Gut. 2023; 72: 1774-82.

4. Chida K, Kawazoe A, Suzuki T, Kawazu M, Ueno T, Takenouchi K, et al. Transcriptomic profiling of MSI-H/dMMR gastrointestinal tumors to identify determinants of responsiveness to anti-PD-1 therapy. Clin Cancer Res. 2022; 28: 2110-7.
5. Al-Rawi DH, Lettera E, Li J, DiBona M, Bakhoum SF. Targeting chromosomal instability in patients with cancer. Nat Rev Clin Oncol. 2024; 21: 645-59.
6. Yang C, Zhao L, Lin Y, Wang S, Ye Y, Shen Z. Improving the efficiency of immune checkpoint inhibitors for metastatic pMMR/MSS colorectal cancer: options and strategies. Crit Rev Oncol Hematol. 2024; 200: 104204.
7. Gonugunta VK, Sakai T, Pokatayev V, Yang K, Wu J, Dobbs N, et al. Trafficking-mediated STING degradation requires sorting to acidified endolysosomes and can be targeted to enhance anti-tumor response. Cell Rep. 2017; 21: 3234-42.
8. Liu S, Kwon M, Mannino M, Yang N, Renda F, Khodjakov A, et al. Nuclear envelope assembly defects link mitotic errors to chromothripsis. Nature. 2018; 561: 551-5.
9. Harding SM, Benci JL, Irianto J, Discher DE, Minn AJ, Greenberg RA. Mitotic progression following DNA damage enables pattern recognition within micronuclei. Nature. 2017; 548: 466-70.
10. Hayman TJ, Baro M, MacNeil T, Phoomak C, Aung TN, Cui W, et al. STING enhances cell death through regulation of reactive oxygen species and DNA damage. Nat Commun. 2021; 12: 2327.
11. Mackenzie KJ, Carroll P, Martin C-A, Murina O, Fluteau A, Simpson DJ, et al. cGAS surveillance of micronuclei links genome instability to innate immunity. Nature. 2017; 548: 461-5.
12. Dou Z, Ghosh K, Vizioli MG, Zhu J, Sen P, Wangensteen KJ, et al. Cytoplasmic chromatin triggers inflammation in senescence and cancer. Nature. 2017; 550: 402-6.
13. Ablasser A, Chen ZJ. cGAS in action: expanding roles in immunity and inflammation. Science. 2019; 363: eaat8657.
14. Gulen MF, Koch U, Haag SM, Schuler F, Apetoh L, Villunger A, et al. Signalling strength determines proapoptotic functions of STING. Nat Commun. 2017; 8: 427.
15. Sun Y, Ji P, Chen T, Zhou X, Yang D, Guo Y, et al. MIIP haploinsufficiency induces chromosomal instability and promotes tumour progression in colorectal cancer. J Pathol. 2017; 241: 67-79.
16. Lin A, Qi C, Wei T, Li M, Cheng Q, Liu Z, et al. CAMOIP: a web server for comprehensive analysis on multi-omics of immunotherapy in pan-cancer. Brief Bioinform. 2022; 23: bbac129.
17. Finotello F, Mayer C, Plattner C, Laschober G, Rieder D, Hackl H, et al. Molecular and pharmacological modulators of the tumor immune contexture revealed by deconvolution of RNA-seq data. Genome Med. 2019; 11: 34.
18. Li T, Fu J, Zeng Z, Cohen D, Li J, Chen Q, et al. TIMER2.0 for analysis of tumor-infiltrating immune cells. Nucleic Acids Res. 2020; 48: W509-14.
19. Dai J, Huang Y-J, He X, Zhao M, Wang X, Liu Z-S, et al. Acetylation blocks cGAS activity and inhibits self-DNA-induced autoimmunity. Cell. 2019; 176: 1447-60.e14.
20. Kumorkiewicz-Jamro A, Pachulicz RJ, Fitter S, Górska R, Duggan J, Vandyke K, et al. *Atriplex hortensis* var. 'rubra' extracts and purified amaranthin-type pigments reduce oxidative stress and inflammatory response in LPS-stimulated RAW264.7 cells. Food Chem. 2025; 462: 140920.
21. Liu Z-S, Cai H, Xue W, Wang M, Xia T, Li W-J, et al. G3BP1 promotes DNA binding and activation of cGAS. Nat Immunol. 2019; 20: 18-28.
22. Sun Y, Hu L, Zheng H, Bagnoli M, Guo Y, Rupaimoole R, et al. MiR-506 inhibits multiple targets in the epithelial-to-mesenchymal transition network and is associated with good prognosis in epithelial ovarian cancer. J Pathol. 2015; 235: 25-36.
23. Lu C, Chen S, Liu S, Liu H, Sun L, Sun Y. Determination of the immunomodulatory role of OTOP2 in colon adenocarcinoma. J Cancer. 2024; 15: 4838-52.
24. Xu J, Gao Y, Ding Y, Feng Y, Chen J, Zhang S, et al. Correlation between Tregs and ICOS-induced M2 macrophages polarization in colorectal cancer progression. Front Oncol. 2024; 14: 1373820.
25. Song SW, Fuller GN, Khan A, Kong S, Shen W, Taylor E, et al. IIp45, an insulin-like growth factor binding protein 2 (IGFBP-2) binding protein, antagonizes IGFBP-2 stimulation of glioma cell invasion. Proc Natl Acad Sci U S A. 2003; 100: 13970-5.
26. Wu Y, Song SW, Sun J, Bruner JM, Fuller GN, Zhang W. IIp45 inhibits cell migration through inhibition of HDAC6. J Biol Chem. 2010; 285: 3554-60.
27. Ji P, Smith SM, Wang Y, Jiang R, Song SW, Li B, et al. Inhibition of gliomagenesis and attenuation of mitotic transition by MIIP. Oncogene. 2010; 29: 3501-8.
28. Wang Y, Hu L, Ji P, Teng F, Tian W, Liu Y, et al. MIIP remodels Rac1-mediated cytoskeleton structure in suppression of endometrial cancer metastasis. J Hematol Oncol. 2016; 9: 112.
29. Chen T, Li J, Xu M, Zhao Q, Hou Y, Yao L, et al. PKCε phosphorylates MIIP and promotes colorectal cancer metastasis through inhibition of RelA deacetylation. Nat Commun. 2017; 8: 939.
30. Sun D, Wang Y, Jiang S, Wang G, Xin Y. MIIP is downregulated in gastric cancer and its forced expression inhibits proliferation and invasion of gastric cancer cells in vitro and in vivo. Onco Targets Ther. 2018; 11: 8951-64.
31. Fang J, Chen Y-L, Yao H-B, Peng S-S, Yang P, Ding Z-Y. MIIP inhibits malignant progression of hepatocellular carcinoma through regulating AKT. Eur Rev Med Pharmacol Sci. 2020; 24: 2335-46.
32. Yan F, Wang Q, Xia M, Ru Y, Hu W, Yan G, et al. MIIP inhibits clear cell renal cell carcinoma proliferation and angiogenesis via negative modulation of the HIF-2α-CYR61 axis. Cancer Biol Med. 2021; 19: 818-35.
33. Gao Y, Fang Y, Huang Y, Ma R, Chen X, Wang F, et al. MIIP functions as a novel ligand for ITGB3 to inhibit angiogenesis and tumorigenesis of triple-negative breast cancer. Cell Death Dis. 2022; 13: 810.
34. Wang Q, Su Y, Sun R, Xiong X, Guo K, Wei M, et al. MIIP downregulation drives colorectal cancer progression through inducing peri-cancerous adipose tissue browning. Cell Biosci. 2024; 14: 12.
35. Yang Q, Guo N, Zhou Y, Chen J, Wei Q, Han M. The role of tumor-associated macrophages (TAMs) in tumor progression and relevant advance in targeted therapy. Acta Pharm Sin B. 2020; 10: 2156-70.

36. Tang Y, Cui G, Liu H, Han Y, Cai C, Feng Z, et al. Converting "cold" to "hot": epigenetics strategies to improve immune therapy effect by regulating tumor-associated immune suppressive cells. Cancer Commun (Lond). 2024; 44: 601-36.
37. Cai J, Song L, Zhang F, Wu S, Zhu G, Zhang P, et al. Targeting SRSF10 might inhibit M2 macrophage polarization and potentiate anti-PD-1 therapy in hepatocellular carcinoma. Cancer Commun (Lond). 2024; 44: 1231-60.
38. Basak U, Sarkar T, Mukherjee S, Chakraborty S, Dutta A, Dutta S, et al. Tumor-associated macrophages: an effective player of the tumor microenvironment. Front Immunol. 2023; 14: 1295257.
39. Huang L, Zhao Y, Shan M, Wang S, Chen J, Liu Z, et al. Targeting crosstalk of STAT3 between tumor-associated M2 macrophages and Tregs in colorectal cancer. Cancer Biol Ther. 2023; 24: 2226418.
40. Wu H, Li J, Yao R, Liu J, Su L, You W. Focusing on the interplay between tumor-associated macrophages and tumor microenvironment: from mechanism to intervention. Theranostics. 2025; 15: 7378-408.
41. Zhang Q, Huang F, Yao Y, Wang J, Wei J, Wu Q, et al. Interaction of transforming growth factor-β-Smads/microRNA-362-3p/CD82 mediated by M2 macrophages promotes the process of epithelial-mesenchymal transition in hepatocellular carcinoma cells. Cancer Sci. 2019; 110: 2507-19.
42. DeNardo DG, Ruffell B. Macrophages as regulators of tumour immunity and immunotherapy. Nat Rev Immunol. 2019; 19: 369-82.
43. Cassetta L, Pollard JW. Targeting macrophages: therapeutic approaches in cancer. Nat Rev Drug Discov. 2018; 17: 887-904.
44. Liu Q, Yang C, Wang S, Shi D, Wei C, Song J, et al. Wnt5a-induced M2 polarization of tumor-associated macrophages via IL-10 promotes colorectal cancer progression. Cell Commun Signal. 2020; 18: 51.
45. Cheng Y, Zhu Y, Xu J, Yang M, Chen P, Xu W, et al. PKN2 in colon cancer cells inhibits M2 phenotype polarization of tumor-associated macrophages via regulating DUSP6-Erk1/2 pathway. Mol Cancer. 2018; 17: 13.
46. Anderson NR, Minutolo NG, Gill S, Klichinsky M. Macrophage-based approaches for cancer immunotherapy. Cancer Res. 2021; 81: 1201-8.
47. Sun Z, Xu Y, Shao B, Dang P, Hu S, Sun H, et al. Exosomal circPOLQ promotes macrophage M2 polarization via activating IL-10/STAT3 axis in a colorectal cancer model. J Immunother Cancer. 2024; 12: e008491.
48. An X, Zhu Y, Zheng T, Wang G, Zhang M, Li J, et al. An analysis of the expression and association with immune cell infiltration of the cGAS/STING pathway in pan-cancer. Mol Ther Nucleic Acids. 2019; 14: 80-9.
49. Bakhoum SF, Ngo B, Laughney AM, Cavallo J-A, Murphy CJ, Ly P, et al. Chromosomal instability drives metastasis through a cytosolic DNA response. Nature. 2018; 553: 467-72.
50. Leghmari K, Bennasser Y, Bahraoui E. HIV-1 Tat protein induces IL-10 production in monocytes by classical and alternative NF-kappaB pathways. Eur J Cell Biol. 2008; 87: 947-62.
51. Burdette DL, Vance RE. STING and the innate immune response to nucleic acids in the cytosol. Nat Immunol. 2013; 14: 19-26.
52. Lan J, Heneghan AF, Sano Y, Jonker MA, Omata J, Xu W, et al. Parenteral nutrition impairs lymphotoxin β receptor signaling via NF-κB. Ann Surg. 2011; 253: 996-1003.
53. Abe T, Barber GN. Cytosolic-DNA-mediated, STING-dependent proinflammatory gene induction necessitates canonical NF-κB activation through TBK1. J Virol. 2014; 88: 5328-41.
54. Chang T-P, Kim M, Vancurova I. Analysis of TGFβ1 and IL-10 transcriptional regulation in CTCL cells by chromatin immunoprecipitation [Internet]. In: Vancurova I, editor. Cytokine bioassays. New York, NY: Springer New York; 2014, p. 329-41. Available from: https://link.springer.com/10.1007/978-1-4939-0928-5_30. (cited 2025 Aug 14).
55. Chang T-P, Poltoratsky V, Vancurova I. Bortezomib inhibits expression of TGF-β1, IL-10, and CXCR4, resulting in decreased survival and migration of cutaneous T cell lymphoma cells. J Immunol. 2015; 194: 2942-53.
56. Gobbi S, Belluti F, Rampa A, Bisi A. Flavonoid-inspired vascular disrupting agents: exploring flavone-8-acetic acid and derivatives in the new century. Molecules. 2021; 26: 4228.
57. Gu J, Liu X, Ji Z, Shen M, Zhu M, Ren Y, et al. Tumor vascular destruction and cGAS-STING activation induced by single drug-loaded nano-micelles for multiple synergistic therapies of cancer. Small. 2023; 19: e2303517.
58. Hong C, Schubert M, Tijhuis AE, Requesens M, Roorda M, van den Brink A, et al. cGAS–STING drives the IL-6-dependent survival of chromosomally instable cancers. Nature. 2022; 607: 366-73.
59. Li J, Hubisz MJ, Earlie EM, Duran MA, Hong C, Varela AA, et al. Non-cell-autonomous cancer progression from chromosomal instability. Nature. 2023; 620: 1080-8.

Cite this article as: Chen S, Lu C, Li J, Shen X, Sun Y. Migration and invasion inhibitory protein inhibits M2 macrophage polarization to suppress colorectal cancer progression through the STING–NFκB2–IL10 axis. Cancer Biol Med. 2026; 23: 86-106. doi: 10.20892/j.issn.2095-3941.2025.0282